

# Scanning tunnelling spectroscopy of electron resonators

Jörg Kliewer\* and Richard Berndt†

*Institut für Experimentelle und Angewandte Physik  
Christian-Albrechts-Universität zu Kiel, D-24098 Kiel, Germany*

S. Crampin‡

*Department of Physics  
University of Bath, Bath BA2 7AY, United Kingdom*

(Dated: February 1, 2008)

The electronic structure of artificial Mn atom arrays on Ag(111) is characterized in detail with scanning tunnelling spectroscopy and spectroscopic imaging at low temperature. We demonstrate the degree to which variations in geometry may be used to control spatial and spectral distributions of surface state electrons confined within the arrays, how these are influenced by atoms placed within the structure and how the ability to induce spectral features at specific energies may be exploited through lineshape analyses to deduce quasiparticle lifetimes near the Fermi level. Through extensive comparison of  $dI/dV$  maps and spectra we demonstrate the utility of a model based upon two-dimensional  $s$ -wave scatterers for describing and predicting the characteristics of specific resonators.

PACS numbers:

## I. INTRODUCTION

A central aim of nanoscale science is to controllably modify material properties on a nanometre scale. One of its greatest achievements has been manipulation of surface atomic structure with the scanning tunnelling microscope (STM) [1], and some of the most striking demonstrations of this capability the construction of complex arrays of adatoms by the maneuvering and positioning of individual adatoms [2]. Synthesized nanoscale structures such as these, as well as other surface nanostructures including islands [3, 4] and step arrays [5] act as resonators for mobile surface electrons, with characteristics that may be controlled by the adjustment of geometrical parameters.

Here we present a detailed analysis of the electronic structure of a particular class of resonator, surface nanocavities constructed from Mn atoms on Ag(111). Of particular interest is the extent to which a simple scattering model, which takes into account the atomic structure of the resonator, can successfully describe its spatial and spectral electron distributions. Recent work [6] has shown that the specific characteristics of individual resonators impact upon the electronic structure of adsorbates positioned within them, and may open up the possibility of atomic scale control of magnetic or chemical properties.

In addition, we consider the use of these artificial

nanoscale structures for probing quasiparticle lifetimes close to the Fermi energy. The lifetimes of excitations enter the description of many important surface phenomena such as the dynamics of charge and energy transfer, and for excitations in surface bands reflect a complex combination of decay processes via both surface-localised and extended states, with the additional influence of screening that varies rapidly as the electron density decreases outside the surface. Successful prediction of lifetimes remains an on-going theoretical problem [7], whilst measurements must overcome considerable challenges (reviewed in Ref. [8]) so that only recently [9] has a consistent account of the lifetime of a prototype quasiparticle, a hole in a surface band, been constructed, based upon tunnelling spectroscopy at the surface state band edge on noble metal (111) faces [10]. The spatial decay of electron interference patterns observed in STM images provides an alternative approach first indicated by Avouris [11], and has been used to measure lifetimes well removed from the Fermi energy  $E_F$  [12]. However, lifetime measurements for states close in energy to  $E_F$  are still lacking but are of particular interest because the relative contributions of phononic and electronic decay channels are expected to change significantly in this range. We indicate how electron resonators may be used for this purpose.

## II. METHODS

### A. Experimental Procedures

We study nanocavities constructed using Mn adatoms on the Ag (111) surface in a custom-built ultra-high

---

\*Present address: Infineon Technologies AG, Postfach 800949, D-81609 München

†Electronic address: berndt@physik.uni-kiel.de

‡Electronic address: s.crampin@bath.ac.uk

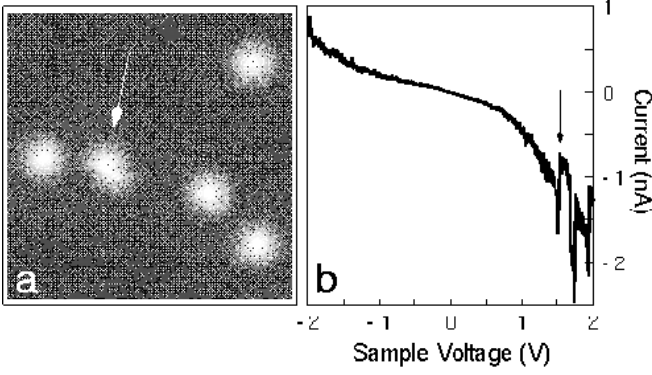


FIG. 1: (a)  $60 \times 60 \text{ \AA}^2$  constant current topograph of Mn adatoms on Ag(111). At  $V = 512 \text{ mV}$  and  $R = 731 \text{ M}\Omega$  the Mn atoms occasionally exhibit tip-induced mobility (arrow). Image scanned at  $1.9 \text{ s/line}$ . (b)  $I/V$  spectrum acquired on top of a single Mn atom. Abrupt current fluctuations occur at  $V = 1.5 \text{ V}$  and  $R = 1 \text{ G}\Omega$ . Spectrum recorded at  $133 \text{ mV/sec}$ , starting at  $V = -2 \text{ V}$ .

vacuum (UHV) STM, operating at a temperature of  $T = 4.6 \text{ K}$  [13]. The Mn atoms were evaporated onto a cold Ag substrate that had been prepared by standard procedures in UHV. Electrochemically etched W tips were prepared in UHV by sputtering and annealing. Differential conductivity ( $dI/dV$ ) spectra were recorded under open feedback loop conditions using a lock-in amplifier with a sinusoidal modulation added to the sample bias. Moreover, maps of  $dI/dV$  were recorded simultaneously with constant current imaging without opening the feedback.

Manganese atoms on Ag(111) image as  $1.6 \text{ \AA}$  high and  $11 \text{ \AA}$  wide protrusions (full width at half maximum) at a sample voltage  $V = 1 \text{ V}$  (Fig. 1a), similar to previous observations of adatom species on noble metal surfaces [2, 14]. Most of the STM images presented here have been recorded at  $V = 1 \text{ V}$  and a tunnelling current  $I = 0.01 \text{ nA}$ , i.e. a tunnelling resistance  $R = 100 \text{ G}\Omega$ ; these values are chosen because the tip-sample interaction is sufficiently strong for  $R$  below  $700 - 750 \text{ M}\Omega$  that atoms are occasionally moved during scans, as demonstrated in Figure 1a. In  $I(V)$  spectroscopy of single Mn atoms we observe abrupt current changes at  $V \approx 1.5 \text{ V}$  and  $R \approx 1 \text{ G}\Omega$ , Figure 1b, indicating the onset of induced atomic mobility. To achieve acceptable signal-to-noise ratios in tunnelling spectroscopy elevated modulation amplitudes were required ( $5 \text{ mV}_{pp}$ ).

We construct artificial structures via controlled relocation of individual Mn atoms, using a sliding process pioneered by Eigler [1]. A Mn adatom is moved by placing the tip over the atom at large tip-sample separation (typically  $R = 100 \text{ G}\Omega$ ), reducing this separation ( $V = 3 \text{ V}$ ,  $R = 500 \text{ M}\Omega$ ) and then moving the tip slowly across the surface (a rate of  $\sim$  one lattice constant per second) to the desired location. The adatom follows the tip motion, and is left in position by retracting the tip.

## B. Modelling

To model the experiments it is important to take into account the constant-current mode of operation that is used in obtaining the  $dI/dV$  maps. The tunnelling current is calculated as [15]

$$I(V, \mathbf{r}) \propto \int_0^{eV} \rho_s(\mathbf{r}, E) T(E, eV, z) dE, \quad (1)$$

where  $\rho_s(\mathbf{r}, E)$  is the local density of states (LDOS) of the sample at the position  $\mathbf{r} = (x, y)$  of the tip and where the transmission probability  $T$  is given by

$$T(E, eV, z) = \exp \left[ -z \sqrt{\frac{4m}{\hbar^2} (\phi_t + \phi_s + eV - 2E)} \right] \quad (2)$$

with tip-sample distance  $z$  and workfunctions  $\phi_t = 4.55 \text{ eV}$  and  $\phi_s = 4.74 \text{ eV}$  of tip and sample respectively [16]. Simulating the feedback loop,  $z$  was adjusted for each lateral position ( $z = z(\mathbf{r})$ ) to ensure constant current  $I$ , which in turn was numerically differentiated to obtain  $dI/dV$ . In using (1) we assume an electronically featureless tip, which is supported by the absence of any tip dependence to be seen during the experiments.

For  $\rho_s$  we consider an array of  $N$  two-dimensional  $s$ -wave scatterers with coordinates  $\mathbf{R}_j$ ,  $j = 0, 1, \dots, N-1$ . This is the model introduced by Heller *et al* [17]. We determine  $\rho_s$  from the Green function

$$\rho_s(\mathbf{r}, E) = -(1/\pi) \text{Im} G(\mathbf{r}, \mathbf{r}; E) \quad (3)$$

which is given by multiple-scattering theory in terms of the free-electron Green function [18]

$$G_0(\mathbf{r}, \mathbf{r}'; E) = -\frac{im^*}{2\hbar^2} H_0^{(1)}(\kappa|\mathbf{r} - \mathbf{r}'|) \quad (4)$$

where  $\kappa = \sqrt{2m^*(E - E_0)/\hbar^2}$  and the  $t$ -matrices that characterise the point scatterers:

$$G(\mathbf{r}, \mathbf{r}'; E) = G_0(\mathbf{r}, \mathbf{r}'; E) + \sum_{j,k} G_0(\mathbf{r}, \mathbf{R}_j; E) T^{jk} G_0(\mathbf{R}_k, \mathbf{r}'; E) \quad (5)$$

$$T^{jk}(E) = t\delta_{jk} + t \sum_{l \neq j} G_0(\mathbf{R}_j, \mathbf{R}_l; E) T^{lk}(E). \quad (6)$$

A number of parameters enter the calculations. We use  $t$ -matrices corresponding to perfectly absorbing scatterers, as identified by Heller *et al.* [17] and used by them to describe the  $dI/dV$  spectrum of a 60 Fe atom corral on Cu(111). This boundary condition reflects the strong coupling to bulk states [19] that occurs at the adatoms. The effective mass  $m^* = 0.42 m_e$  and surface state band edge  $E_0 = -67 \text{ meV}$  have been determined previously [9, 20]. The positions of the atoms and the

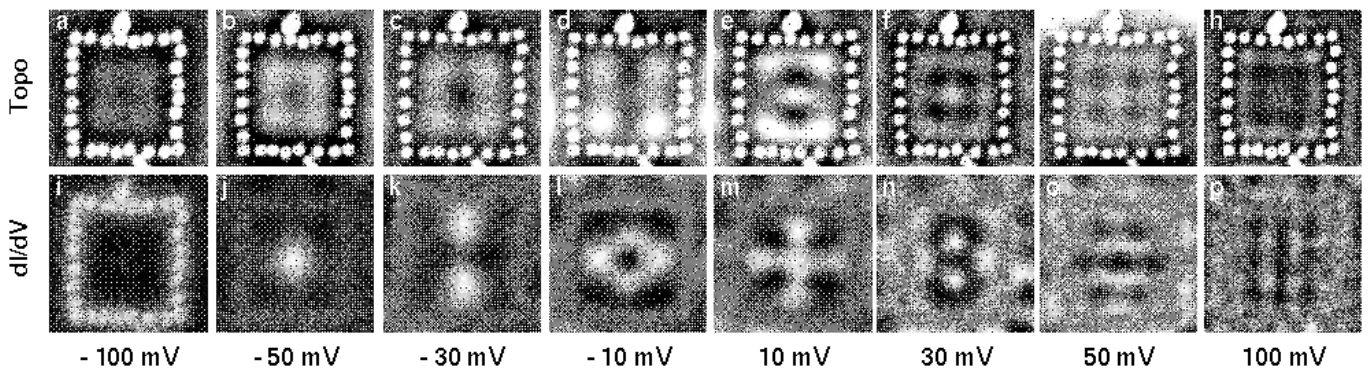


FIG. 2: Array of 28 Mn atoms forming a rectangle of size  $\approx 90 \times 100 \text{ \AA}^2$ . Panels (a)–(h) show constant current topographs recorded at the indicated sample voltages. Panels (i)–(p) are  $dI/dV$  maps recorded simultaneously.

lateral position of the tip are crucial in determining the exact shape of  $dI/dV$  spectra. For example, only the highest symmetry eigenstates contribute at the centre of a circular structure, but slightly off centre or if the shape is not exactly regular a mixing of state occurs, giving additional structure. Uncertainty enters these coordinates through the piezo calibration and possible anisotropy of the piezo sensitivity in the fast ( $x$ ) and slow ( $y$ ) scanning directions. Therefore an optimisation scheme was used based upon a  $\chi^2$  fit using the Levenberg-Marquardt method in which the relative coordinates were fixed but independently scaled in the  $x$  and  $y$  directions. After the initial determination, the piezo calibration parameters were held fixed in all subsequent calculations. In a second stage, the calculations have been extended further to include an energy dependent lifetime of the electronic states (Sect. III D). This was accomplished via a parameterised imaginary self energy  $i\Sigma(E)$  added to the energy  $E$  in computing  $G$  from equations (4)–(6). The importance of the self energy in determining the peak amplitudes and widths in the LDOS has been noted previously [19, 21]. Here we exploit this dependence to extract  $\Sigma$  from experimental data.

### III. RESULTS

#### A. 28 atom rectangle

Figure 2 displays data from an array of 28 Mn adatoms. Images a–h are constant current topographs covering a range of different voltages, recorded at values indicated in the figure. The adatoms, which appear as bright protrusions in every case, have been arranged into a rectangular geometry with approximate dimensions of  $90 \times 100 \text{ \AA}^2$ . Inside this structure a weak corrugation is found, originating from the confinement of the surface state electrons. A nonlinear height scale has been used for display, in order to render this weak corrugation easily discernible; this has the side effect that the adatoms appear rather blunt. At negative voltages (i.e. when tunnelling from occupied levels in the sample) the constant current

topographs exhibit a rectangular pattern of four maxima within the confining array of Mn atoms, which is still discernible at voltages well below the bottom of the surface state band at  $E_0 = -67 \text{ meV}$ . This pattern persists owing to the preferential tunnelling from occupied states at the Fermi level. At positive voltages, imaging unoccupied states, the pattern becomes more complex and varies with  $V$ , the most significant tunnelling now occurring at energies corresponding to the varying bias voltage.

Images i–p show  $dI/dV$  maps that were recorded simultaneously with the topographic scans. Below  $E_0$ , the adatoms cause clear features, whereas no corrugation is discernible inside the array. In contrast, above  $E_0$  a clear wave pattern arises within the structure, while the adatoms are only weak features which conveniently serve to indicate the rectangular boundary. The evolution with energy of the internal pattern is as expected, representing a progression through the nodal structures of the lowest lying “particle-in-a-box” eigenstates of the rectangular cavity,  $|\psi_{n,m}(x,y)|^2 \propto |\sin(n\pi x/X) \sin(m\pi y/Y)|^2$  where  $X$  and  $Y$  are the linear dimensions of the structure. At low energy, Fig. 2j, a single maximum occurs ( $n,m = 1,1$ ). Next, two maxima appear along the longer axis of the rectangle (Fig. 2k), corresponding to the  $n,m = 1,2$  level. The  $-10 \text{ mV}$  map (Fig. 2l) showing four maxima, two along each axis of the rectangle, reflects contributions from both the second ( $n,m = 1,2$ ) and third ( $n,m = 2,1$ ) levels. The states are in reality resonances that in general overlap in energy, so that  $dI/dV$  maps can contain contributions from several. At higher energies, the pattern becomes increasingly complex.

Calculated results are displayed in Fig. 3 where panels a–g are topographs, h–n are  $dI/dV$  maps and o–u are LDOS maps. Close inspection and comparison with Figs. 2b–h, and 2j–p reveals that the experimental features are reproduced well by the model calculations. As pointed out previously [20], experimental  $dI/dV$  data recorded by the methods used here are affected by the variations in tip-sample separation which give rise to the corrugation in the topographs. Consequently  $dI/dV$  maps are not directly comparable to LDOS maps, a fact clearly

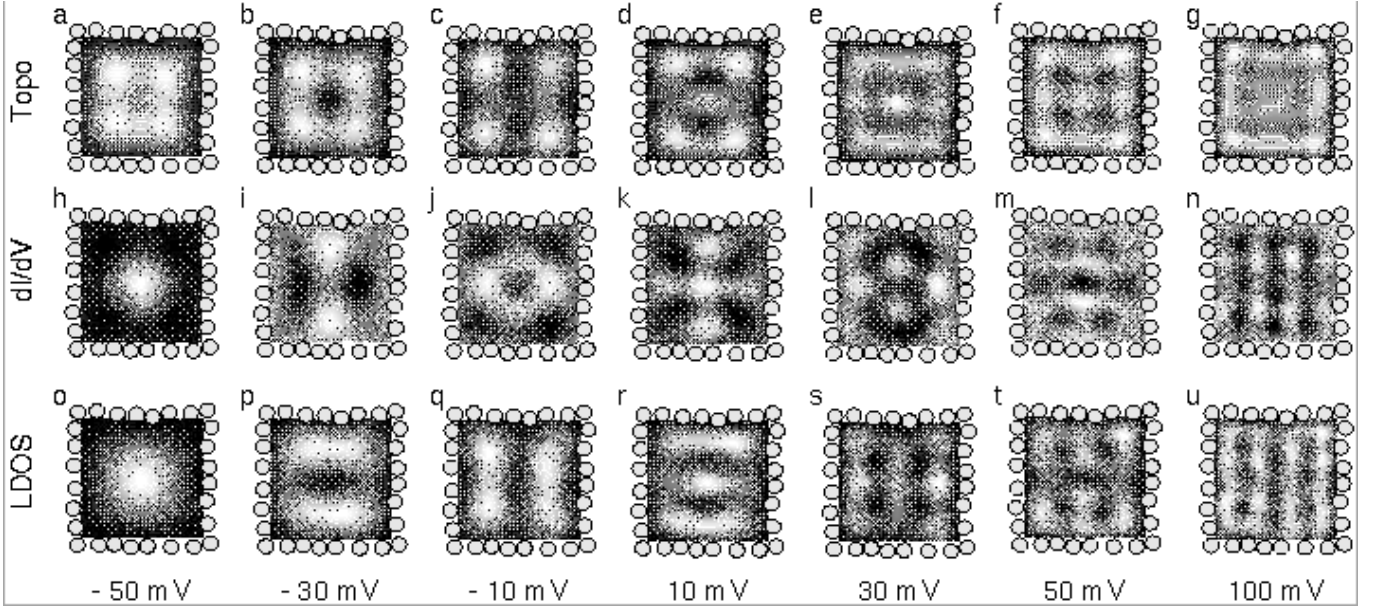


FIG. 3: Calculated results for the 28 atom rectangle. (a)–(g) topographs, (h)–(n)  $dI/dV$  maps, (o)–(u) LDOS.

visible by comparing Figs. 3l and s, or 3m and t, although the similarity between the two tends to increase with increasing bias voltages. Indeed, around zero bias it is topographs and not  $dI/dV$  that are expected to resemble the LDOS, and this is clearly the case in Fig. 3.

A more detailed comparison between experiment and theory is possible in the case of  $dI/dV$  spectra. An example measured near the centre of the rectangular resonator is shown in the left panel of Fig. 4. Tunneling from a  $s$ -state tip directly at the centre of an ideal rectangular structure can only take place into surface state levels with odd quantum numbers  $n, m$ . This is the origin of the large peaks at  $-50$  meV and between 0 and 40 meV. Irregularities in the structure and deviations in position of the tip from the exact centre introduce additional weak tunneling channels, e.g. near  $-25$  meV, whilst the intrinsic width of the confined levels further modifies the

spectrum. Comparing the measured spectrum with the LDOS calculated using the two-dimensional scattering model that includes the structural irregularities and correct tip position, displayed in the same panel in Fig. 4, we see the latter faithfully reproduces the differential conductivity spectrum. Note that the characteristic temperature associated with Kondo behaviour in Mn/Ag alloys is  $T_K \simeq 40$  mK [22] and thus does not affect the line shape [23] under the present experimental conditions.

### B. 35 atom ring

We have also performed similar experiments and calculations on other geometries, such as adatom rings. The right panel of Figure 4 contains a comparison between the differential conductivity spectrum, measured approximately  $5$  Å off centre in a  $220$  Å diameter ring formed from 35 Mn adatoms, and the corresponding LDOS obtained using the  $s$ -wave scattering model. The spectrum contains a large number of peaks, the off-centre position enabling low symmetry eigenstates to provide channels for tunnelling, but these are reproduced in the theoretical LDOS spectrum calculated using the precise atomic positions of the Mn ring. We conclude that the  $s$ -wave scattering model provides an adequate basis for modelling the spatial and spectral electron distributions in electron resonators.

### C. Adatoms in resonators

Having characterised the properties of electron resonators we have next investigated the interaction with

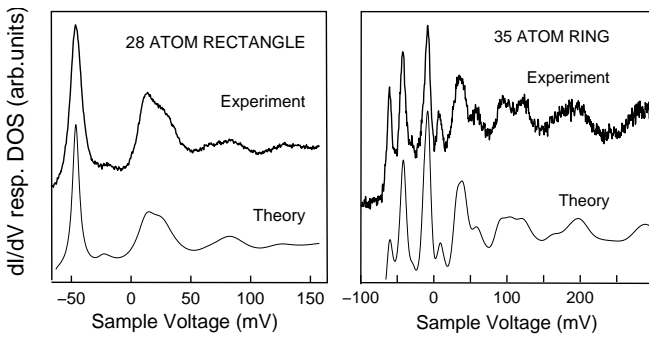


FIG. 4: Left: Measured  $dI/dV$  spectrum and calculated LDOS of the 28 atom rectangle. Right:  $dI/dV$  spectrum and theoretical LDOS of a  $220$  Å diameter ring of 35 Mn adatoms.

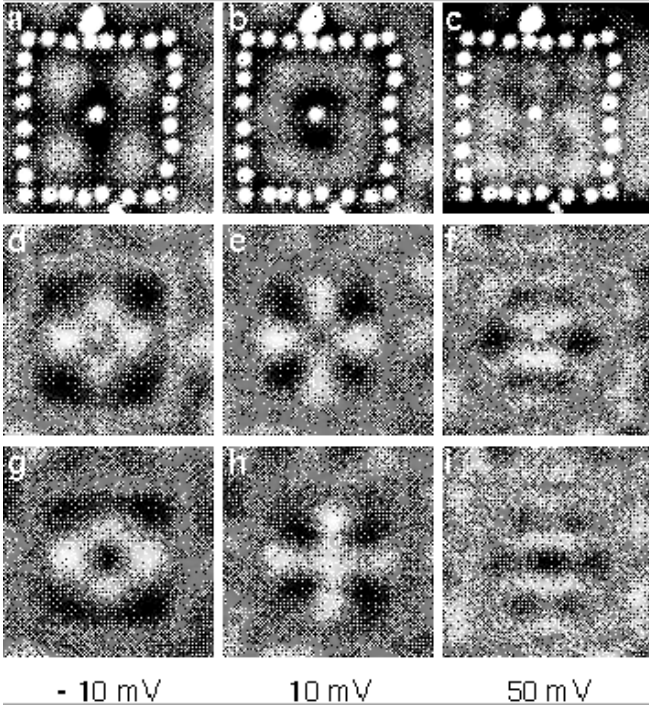


FIG. 5: Topographs of a 28 atom rectangle with a central Mn adatom recorded at the indicated sample voltages (a-c, top row), and  $dI/dV$  maps of the same structure with (d-f, middle row) and without (g-i, bottom row) the central atom.

an additional atom introduced into the nanocavity region. These structures were formed by maneuvering one of the boundary Mn atoms into the central region, and then moving a Mn atom elsewhere on the surface into the vacant position in the boundary, restoring the integrity of the resonator.

In Figure 5 we show  $dI/dV$  maps of a rectangular structure made from 28 Mn atoms and measured at three different voltages, contrasting the images obtained with and without a Mn atom inside the structure. At first glance the presence of the central atom appears to barely affect the wave pattern inside the rectangle, apart from in the immediate vicinity of the centre atom. There, the difference is striking. At voltages of  $V = -10$  mV and  $V = 50$  mV where  $dI/dV$  is at a minimum in the empty structure (Figs. 5g and i),  $dI/dV$  exhibits a peak in the centre upon insertion of the atom (Figs. 5d and f). At  $V = 10$  mV, however, the maximum observed in the empty rectangle (Fig. 5h) changes to a minimum (Fig. 5e).

This “contrast reversal” has been previously reported and explained as a consequence of the strong hybridisation between states on the Mn atom and substrate surface electron levels [6], and has been reproduced in calculations of the local density of states directly on Mn atoms in resonators of various geometries using full three-dimensional multiple scattering calculations. Here we consider how this interaction extends away from the central Mn atom and the degree to which the two-

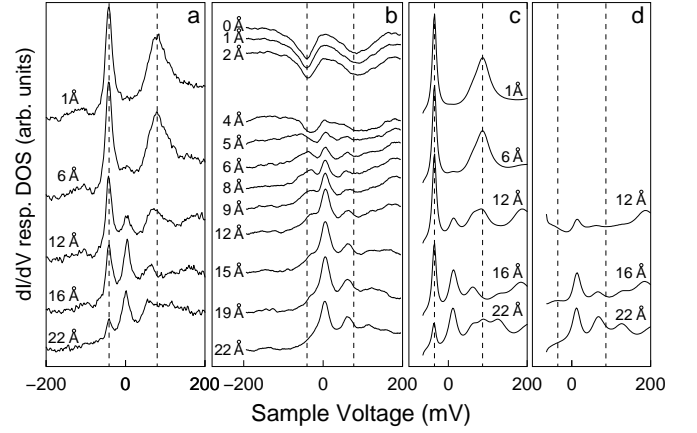


FIG. 6: Evolution of recorded  $dI/dV$  spectra with increasing lateral distance from the centre of a 16 Mn atom ring radius  $\sim 40$  Å (a) without and (b) with a central Mn atom, and spectra calculated using the two-dimensional scattering model of the LDOS for the same systems, (c) without and (d) with the central atom. The vertical dashed lines mark the energies of the main spectral features present at the centre of the empty structure.

dimensional scattering model describes the behaviour. Fig. 6 shows a series of  $dI/dV$  spectra measured at various distances from the centre of an empty adatom ring, and when a Mn atom has been introduced. Also shown are the LDOS calculations for identical geometries. Comparing  $dI/dV$  spectra in Figs. 6a and b at central positions closest to the location of the new adatom, it is clear that spectral peaks in the empty resonator coincide with troughs of the occupied structure (vertical dashed lines). This is evidence for strong hybridisation [6]. Moving laterally away from this central position the characteristic peak structure of the empty resonator returns, with the exception of the lowest peak near  $-40$  mV which remains absent even at large displacements. This prominent feature is associated with a nodeless resonator eigenstate that has its maximum at the centre of the ring, and so is particularly sensitive to the introduction of a Mn atom into the central region.

The two right-most panels in Fig. 6 show the LDOS calculated for this system using the two-dimensional scattering model, at lateral positions at which  $dI/dV$  spectra were recorded. The prominent features in the experimental spectra are reproduced well in the theoretical curves, again showing that the simple scattering model, using the exact atomic locations of the Mn atoms making up the structure, gives an accurate and valid account of the electronic structure of resonators. The calculations also confirm that the dominant state in the empty resonator is absent in the spectrum of states of the occupied resonator, so that the insensitivity of  $dI/dV$  maps to the presence of the central atom away from its immediate vicinity that was suggested by Fig. 5 clearly does not extend to all sample voltages. Note that in Fig. 6d we have omitted theoretical spectra within 10 Å of the cen-

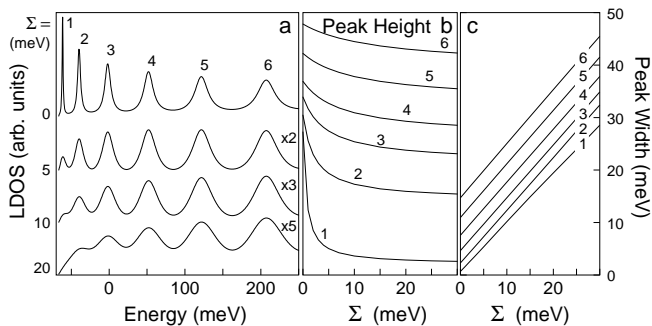


FIG. 7: Effect of a constant imaginary part  $\Sigma$  of the self energy on the LDOS of a 36 atom circle with 210 Å diameter. (a) Calculated LDOS at the centre for various  $\Sigma$  indicated in the figure. Variation of peak (b) heights and (c) widths with  $\Sigma$ .

tral Mn atom. Within this radius (which is much greater than the topographic radius of the Mn atoms) the differential conductivity also has large contributions from channels involving bulk states scattered by the adatom [24], and these are not included in the model. Also omitted in the model is any spatial information about the adatom orbitals that would also be required to model  $dI/dV$  spectra (and maps) in its immediate vicinity.

#### D. Energy dependent self energy

The basic idea of our approach to lifetime measurements is straightforward [13]. Exploiting the properties of the electron resonators identified in the previous sections we construct nanocavities with electronic features in the vicinity of  $E_F$ . The lineshape of the spectral features are affected by lifetime-limiting processes so that through analysis the lifetime  $\tau$  can be determined. By changing the geometry of nanoscale structures it is possible to tune the eigenstate energies of the structures, and thus generate states at various energies in order to obtain the energy dependence of the lifetime. The two-dimensional scattering model validated above enables the design of suitable structures. We note that a fully quantitative analysis will also require information on the energy dependence of the tip density of states, which is not expected to be constant over a wide energy range, and likewise the bulk density of states of the crystal which causes a background signal in  $dI/dV$  spectra. Here, we seek to demonstrate the concept and so neglect these influences. Following Li et al. [10] we describe the lifetime effects in terms of an effective imaginary part  $\Sigma$  of the self energy, where  $\tau = \hbar/(2\Sigma)$ .

The effect of  $\Sigma$  on the LDOS of an artificial nanoscale resonator is shown in Fig. 7a for a 210 Å diameter ring. The calculation for vanishing  $\Sigma$ , i.e. infinite lifetime, yields a series of sharp resonances (Fig. 7a, top curve). Note that the spectrum corresponds to the centre of the structure. The high symmetry gives the “cleanest” spectrum, avoiding difficulties that exist at off-centre po-

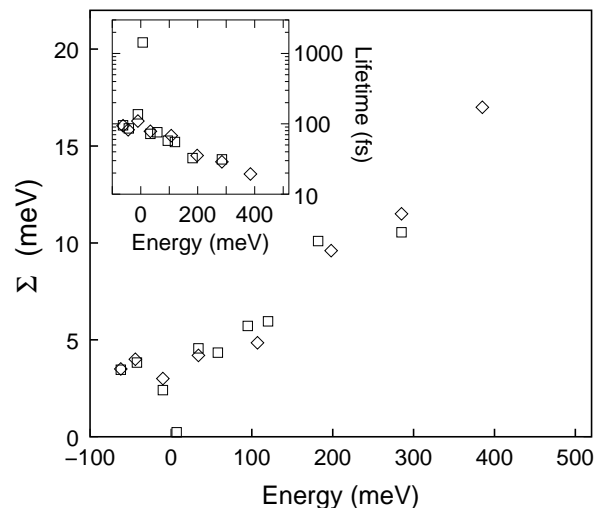


FIG. 8:  $\Sigma(E)$  extracted from analysis of  $dI/dV$  spectra of a 115 Å radius 35 atom circular resonator (diamonds, squares) and a 40 Å radius 16 atom circular resonator. The  $\Sigma$  values are plotted at the position of the respective spectral features. The inset shows the equivalent lifetimes  $\tau = \hbar/(2\Sigma)$  of hot holes and electrons.

sitions where resonances can overlap. With increasing  $\Sigma$  there is a reduction of the peak heights and a concomitant broadening, especially apparent for the lowest of the states which have the sharpest intrinsic profile. These trends are quantified by fitting a series of Lorentzians to the data, and Figure 7b and c display the widths and height extracted through this analysis. As  $\Sigma$  increases, the peak heights decrease monotonically, the lowest (in energy) peaks most rapidly, whilst there is an essentially linear dependence of the peak width on  $\Sigma$ .

Figure 8 shows values of  $\Sigma(E)$  obtained from an analysis of measurements from two nanostructures. For each,  $\chi^2$  fits were made over limited energy ranges ( $\sim 100$  meV) adjusting coefficients of a linear parameterisation of  $\Sigma$ . We estimate the error of  $\Sigma$  thus determined to be of the order of  $\pm 30\%$ . The diamonds and squares are derived from  $dI/dV$  spectra for a 35 atom circular resonator, and the filled circles were obtained from a 16 atom circle. Below the Fermi energy ( $E = 0$ )  $\Sigma$  approaches a value obtained previously from spectra taken on clean terraces which yielded  $\Sigma = 3$  meV [9]. There is a clear increase of  $\Sigma$  at large energies, and we find  $\Sigma(E = 0.5 \text{ eV}) \sim 20$  meV, which is comparable with an extrapolation down to this energy of data for the Ag(111) surface state extracted from the spatial coherence of interference patterns at energies  $E > 1$  eV by Bürgi *et al.* [12]. Finally, at energies close to  $E_F$  we observe a marked decrease of  $\Sigma$  which corresponds to an increased lifetime of the corresponding quasiparticles (inset in Fig. 8). Increased lifetimes are indeed expected as both the phononic and electronic decay channels become less efficient. While further data close to  $E_F$  is necessary to quantitatively characterize this effect the first results are encouraging. Future work will also address the relation



of the self-energies determined from atomic arrays to that of an unperturbed surface. We note that data from resonators of different diameters (40 Å and 115 Å) yield similar  $\Sigma(E)$ . This similarity appears to indicate that the influence of the array may be rather small.

#### IV. SUMMARY

Using scanning tunnelling spectroscopy and spectroscopic imaging at low temperature we have investigated artificial Mn atom arrays on Ag(111). These act as electron resonators and we have demonstrated the degree to which variations in geometry may be used to control spatial and spectral distributions of confined surface state

electrons. This control may be exploited in manipulating the local density of states of adsorbates introduced into the resonator, or as we have demonstrated, to generate spectral features at specific energies in order to perform lineshape analyses from which quasiparticle lifetimes may be deduced. Extensive comparison of  $dI/dV$  maps and spectra indicated the utility of a model based upon two-dimensional  $s$ -wave scatterers for describing and predicting the characteristics of specific resonators.

#### Acknowledgements

This work has been supported the DFG, the DAAD and the UK EPSRC.

- 
- [1] D. M. Eigler, E. K. Schweizer, *Nature* **344**, 524 (1990).
  - [2] M. F. Crommie, C. P. Lutz, D. M. Eigler, *Science* **262**, 218 (1993).
  - [3] Ph. Avouris, I.-W. Lyo, *Science* **264**, 942 (1994).
  - [4] J. Li, W.-D. Schneider, R. Berndt, S. Crampin, *Phys. Rev. Lett.* **80**, 3332 (1998).
  - [5] L. Bürgi, O. Jeandupeux, A. Hirstein, H. Brune, K. Kern, *Phys. Rev. Lett.* **81**, 5370 (1998).
  - [6] J. Kliewer, S. Crampin, R. Berndt, *Phys. Rev. Lett.* **85**, 4936 (2000).
  - [7] P.M. Echenique, J. Osma, V.M. Silkin, E.V. Chulkov, J.M. Pitarke, *Appl. Phys. A* **71**, 503 (2000).
  - [8] R. Matzdorf, *Surf. Sci. Rep.* **30**, 153 (1998).
  - [9] J. Kliewer, R. Berndt, E. V. Chulkov, V. M. Silkin, P. M. Echenique, S. Crampin, *Science* **288**, 1399 (2000).
  - [10] J. Li, W.-D. Schneider, R. Berndt, O. R. Bryant, S. Crampin, *Phys. Rev. Lett.* **81**, 4464 (1998).
  - [11] Ph. Avouris, I.-W. Lyo, R. E. Walkup, Y. Hasegawa, *J. Vac. Sci. Technol. B* **12**, 1447 (1994).
  - [12] L. Bürgi, O. Jeandupeux, H. Brune, K. Kern, *Phys. Rev. Lett.* **82**, 4516 (1999).
  - [13] J. Kliewer, PhD thesis, RWTH Aachen, D-52056 Aachen, Germany (2000).
  - [14] M. F. Crommie, C. P. Lutz, D. M. Eigler, *Phys. Rev. B* **48**, 2851 (1993).
  - [15] A. Selloni, P. Carnevali, E. Tosatti, C. D. Chen, *Phys. Rev. B* **31**, 2602 (1985).
  - [16] H. B. Michaelson, *J. Appl. Phys.* **48**, 4729 (1977).
  - [17] E. J. Heller, M. F. Crommie, C. P. Lutz, D. M. Eigler, *Nature* **369**, 464 (1994).
  - [18] E.N. Economou, *Green's Functions for Quantum Physics* (Springer-Verlag, Berlin, 1983).
  - [19] S. Crampin, M. H. Boon, J. E. Inglesfield, *Phys. Rev. Lett.* **73**, 1015 (1994).
  - [20] J. T. Li, W.-D. Schneider, R. Berndt, *Phys. Rev. B* **56**, 7656 (1997).
  - [21] S. Crampin, O. R. Bryant, *Phys. Rev. B* **54**, R17367 (1996).
  - [22] J. Flouquet, *Phys. Rev. Lett.* **25**, 288 (1970).
  - [23] J. Li, W.-D. Schneider, R. Berndt and B. Delley, *Phys. Rev. Lett.* **80**, 2893 (1998).
  - [24] S. Crampin, *J. Phys.: Condens. Matter* **6**, L613 (1994).